



# Structure Optimization and Modal Parameter Identification of Wing Rib Beam Based on Hammering Modal Test

Chunping Wu, Shiwei Zhao\*, Daochun Li, Fengshuo Zhang and Yongkang Li<sup>1</sup>

School of Aeronautic Science and Engineering, Beihang University, No. 37, Academy Road, Haidian District, Beijing, China

\*Corresponding author E-mail: shiweizhao@buaa.edu.cn

**Abstract.** Model optimization has an important influence on the accuracy of simulation results based on finite element models. Existing research have been carried out various ideas for model correction to make the finite element model consistent with reality and easy for engineering practice. Good results have been achieved, but there are not too many researches based on the optimization of aircraft structure. In this paper, the finite element model of the wing rib beam structure is corrected by hammering modal experiment results, and on the basis of the optimized finite element model, the modal parameter identification is carried out for the wing rib beam structure by the NExT-ERA, and the results show that the identification results by the NExT-ERA are in good consistence with the finite element simulation results.

**Keywords:** structure optimization, modal parameter identification, hammering modal test.

## 1 Introduction

Model correction is the core of structural dynamics model validation <sup>[1]</sup>, which is a key link to ensure the reliability of structural simulation results. Model correction methods can be roughly divided into two categories: matrix method and parametric method, and the parametric method is commonly used for finite element model correction due to its specific physical meaning, which has been widely used in aerospace field.

There have been many research results in the field of model correction, He et al. <sup>[2]</sup> proposed a model correction and virtual validation method considering modeling uncertainty, which showed that the corrected finite element model has high accuracy and reliability. Wan et al. <sup>[3]</sup> proposed a structural damage identification method based on the combination of modal flexibility curvature and Bayesian-based finite element model correction, which achieves the precise location of damage and the identification of damage extent. Li et al. <sup>[4]</sup> proposed a dynamic model updating method for structures with automatic mode recognition. The effectiveness of the proposed model updating method is verified by using the intrinsic frequency and mode shapes of the plate

obtained from experimental modal analysis as the updating target of the finite element model. She et al. [5] proposed a neural network finite element model correction method based on genetic algorithm optimization can effectively improve the efficiency and accuracy of finite element model correction. Xu et al. [6] carried out finite element model modification as well as modal optimization of Z-pipe based on the response surface method, and achieved the design goal of keeping the structure low-order intrinsic frequency away from the resonance point by modifying the material parameters through multi-objective optimization with the help of vibration sweep test data, Zhu et al. [7] verified the validity of the solar wing drive mechanism model, and realized the design of the structural strength in accordance with the safety margin.

Existing studies have dealt less with finite element model corrections for aircraft structures, In this paper, the finite element model of the wing rib beam structure is optimized by the results of the hammering modal experiment, and based on the response results of the optimized finite element model, the frequency and mode shapes of the structure are identified by the time-domain modal identification method named NExT-ERA(Natural Excitation Technique and Eigensystem Realization Algorithm), so as to lay the foundation for the health monitoring based on the structural modal vibration shapes.

## 2 Optimization of the Wing Rib Beam Structure

### 2.1 The Parameter of the Wing Rib Beam Structure

The rib beam has the length of  $2m$ , the width of  $0.1m$  and the thickness of  $0.25m$ . Ten grooves distribute on the two faces of the rib beam, and the outer size for each groove is  $45cm \times 9cm \times 1cm$ , the thickness of the outer edge of the groove is  $0.5cm$ . The size of the fixed rectangular body is  $120cm \times 120cm \times 30cm$ , and nine through-holes with the diameter  $12cm$  arrange on the rectangular body uniformly for fixation. The rib beam structure is symmetrical on the middle face, the thickness of the middle face is  $0.5cm$ , and each groove has the hole in the middle with  $5cm$  length and  $1cm$  radius as shown in Figure 1. The density, modulus of elasticity ( $E$ ) and Poisson's ratio ( $\nu$ ) of the structure are  $2700kg/m^3$ ,  $7e10$  and  $0.3$  respectively.

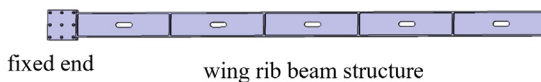


Fig. 1. Schematic diagram of wing rib beam structure.

### 2.2 Modal Experiments Based on the Hammering Method

The wing rib beam is fixed on the test ground base, and acceleration sensors are arranged at different positions on the structure, the acceleration response of the structure

is obtained through the acceleration sensors after the hammering, and the frequency response function of the structure is obtained through the Testlab2019.1, which can obtain the intrinsic frequency, damping ratio, and mode vibration shapes, and the finite element model is optimized based on the results of the hammering experiment.

The three-degree-of-freedom accelerometers are arranged two by two uniformly symmetrical on the wing rib beam structure, as shown in Figure 2 and Figure 3.



Fig. 2. Position of the acceleration sensor and the overall coordinate system.

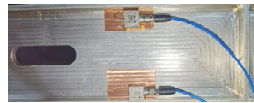


Fig. 3. Acceleration sensor.

In the Geometry module of the Testlab2019.1, ten points are used to construct a simplified model of the structure as in Figure 4, with point one to eight corresponding to the sensor positions on the structure. The nine and ten points serve as the fixed ends of the structure with the coordinate (0,0,0) and (0,10,0).

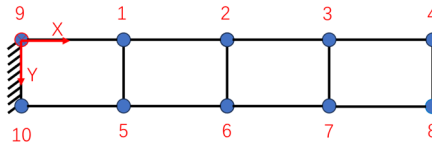


Fig. 4. Diagram of coordinate system and eight sensors.

According to the specific dimensions of the structural and the sensor mounting position, the coordinates of each point are shown in Table 1.

Table 1. Coordinates of ten points.

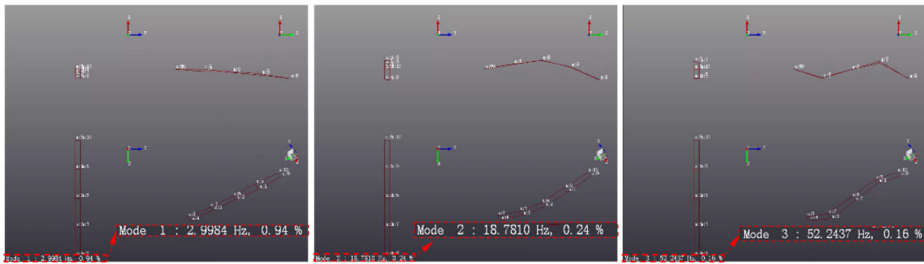
Point	Coordinate ( <i>cm</i> )	
	(X,Y,Z)	(X,Y,Z)
1	(50,0,0)	6 (100,10,0)
2	(100,0,0)	7 (150,10,0)
3	(150,0,0)	8 (200,10,0)
4	(200,0,0)	9 (0,0,0)
5	(50,10,0)	10 (0,10,0)

According to the overall coordinate system arrangement set by wing rib beam, the three-degree-of-freedom orientation configuration of the acceleration sensors is completed in the Impact Testing module of the Testlab2019.1 software as shown in Table 2.

The force hammer was connected to the channel of the data acquisition system, and the same channel configuration was performed in Impact Testing, where the force hammer was used to perform hammering experiments to obtain the intrinsic frequencies of the structure, and the corresponding modal vibration patterns. The results are shown in Figure 5 to Figure 6.

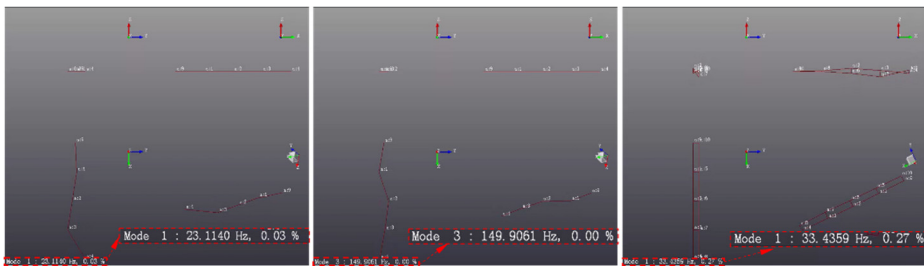
**Table 2.** Sensor configuration based on overall coordinate system orientation.

Sensor number	Overall coordinate system orientation						
	X	Y	Z	X	Y	Z	
<b>Sensor orientation configuration</b>							
1	X	Y	-Z	5	X	Y	Z
2	X	Z	-Y	6	X	Y	Z
3	X	Y	-Z	7	X	Y	Z
4	X	Y	-Z	8	X	Z	-Y



(a) First-order bending mode (b) Second-order bending mode (c) Third-order bending mode

**Fig. 5.** Mode parameters in the Z-X vibration plane.



(a) First-order bending mode (b) Second-order bending mode (c) First-order torsion mode

**Fig. 6.** Mode parameters in the X-Y vibration plane and first-order torsion mode.

### 2.3 Finite Element Model Optimization

Based on the Abaqus, the intrinsic frequency and mode shapes of the structural finite element model are obtained, as shown in Figure 7.

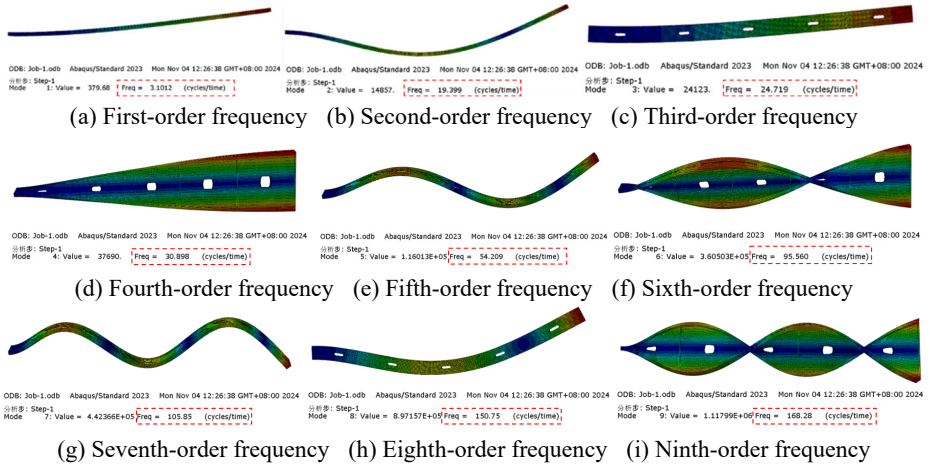


Fig. 7. Abaqus modal analysis results.

The modal analysis shows that the first nine orders of modal vibrations of the structure contain a total of three orders of torsional mode vibrations and six orders of bending mode vibrations, and the results of Abaqus simulation and the results from the hammering experiments are summarized in Table 3, and the errors between the two are calculated.

Table 3. Comparison of intrinsic frequencies.

Vibration plane	Order	Abaqus	Hammering	Errors
Z-X	1	3.1012 Hz	2.9984	3.4%
	2	19.399 Hz	18.7810	3.3%
	3	54.209 Hz	52.2437	3.7%
X-Y	1	24.719 Hz	23.1140	6.9%
	2	150.75 Hz	149.9061	1%
Torsion mode	1	30.898 Hz	33.4359	7.6%

(Errors=abs(Abaqus-Hammering)/Hammering × 100%)

From the analysis in the table, it can be seen that the error between the intrinsic frequency of the bending mode of the Z-X plane obtained by the hammering method and the Abaqus simulation results are kept within the error of 5%, the bending mode of the X-Y plane and the torsion mode is not greater than 8%. Optimum finite element model based on the hammering experimental results so that the results of the finite element model are as consistent as possible with the experimental values.

### 3 Identification of Modal Parameters of the Wing Rib Beam Structure

#### 3.1 Identification of Bending Mode Parameters on Z-X Vibration Plane

The dynamic response simulation of the optimized finite element structural model is carried out by Abaqus, and the two-order bending mode shapes of the Z-X vibration planes are identified by the NEX-T-ERA, as shown in Figure 8, in which the simulated values are obtained by the Abaqus modal analysis.

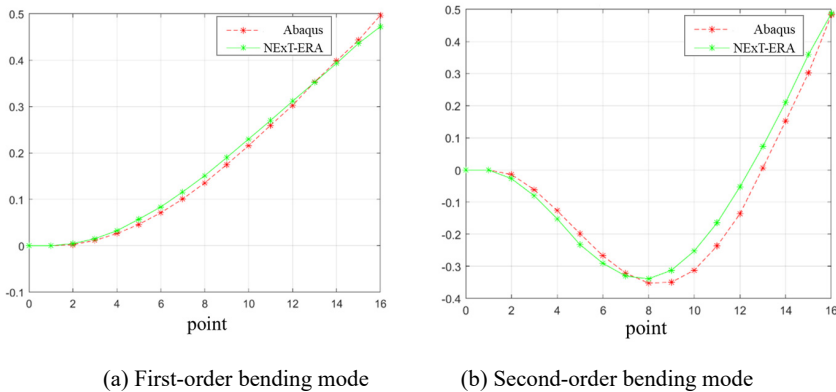


**Fig. 8.** Bending mode shapes in the X-Y vibration plane.

The frequency errors for the simulated values by Abaqus and the identified values by NEX-T-ERA are shown in Table 4, and the vibrational mode correlation is represented by the MAC as in Table 5.

**Table 4.** Comparison of Abaqus simulated values and NEX-T-ERA identified values.

Frequency (Hz)	Abaqus	NEX-T-ERA	Errors
First-order bending mode	3.1012	2.9301	5.5%
Second-order bending mode	19.399	19.4343	0.2%

$$(\text{Errors}=\text{abs}(\text{Abaqus}-\text{NEX-T-ERA})/\text{Abaqus} \times 100\%)$$

**Table 5.** MAC of the first two orders of bending mode shapes.

Bending mode shapes	MAC
First-order	0.9989
Second-order	0.9842

From the comparison of obtained bending intrinsic frequencies and the MAC of the associated modal shapes, the modal shapes and intrinsic frequencies of the first two orders are in good agreement with the Abaqus simulation results.

### 3.2 Identification of Torsional Mode Parameters

Based on the time response data of points in the two prongs on the Y-Z vibration plane as shown in Figure 9. The torsional mode shapes of the structure obtained by the NEXT-ERA are shown in Figure 10, and the identified torsional shapes and intrinsic frequency are verified against the simulation values, as shown in Table 6 and Table 7.

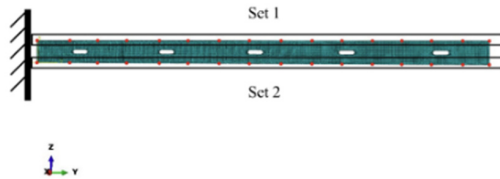
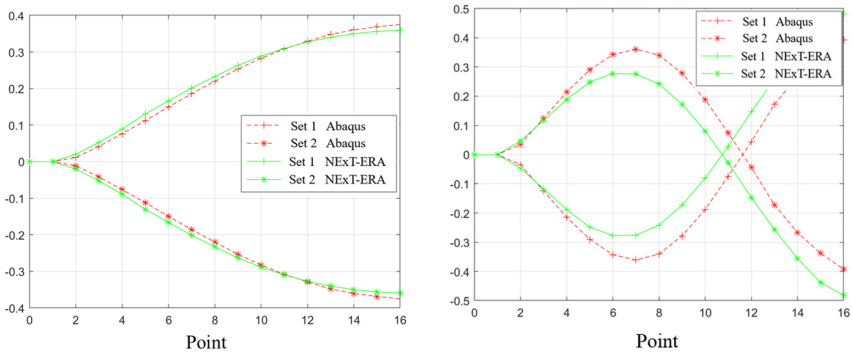


Fig. 9. Data points on the wing rib beam structure.



(a) First-order torsional mode shape

(b) Second-order torsional mode shape

Fig. 10. The torsional mode shapes.

Table 6. Comparison of Abaqus simulated values and NEXT-ERA identified values.

Frequency (Hz)	Abaqus	NEXT-ERA	Errors
First-order torsional mode	30.898	31.2073	1%
Second-order torsional mode	95.560	99.2755	3.9%

Table 7. MAC of the first two orders of torsional mode shapes.

torsional mode shapes	MAC
First-order	0.9990
Second-order	0.9497

From the analysis results in the table, it can be seen that for the first two orders of the torsional intrinsic frequency and torsional mode shapes, the errors between the Abaqus simulation values and the NEXT-ERA identified values are less than 4%, and the similarity of the first two orders of the torsional mode shapes is more than 0.9,

which shows that the NExT-ERA has a great accuracy in the identification of torsional intrinsic frequency and mode shapes of the wing rib beam structure.

## 4 Conclusions

In this paper, the finite element model of the wing rib beam structure is optimized based on the results of hammering experiments, and the modal parameters are identified based on the optimized model response data by the NExT-ERA, and the identification results are in good agreement with the Abaqus simulation results.

## References

1. Ding Jifeng, Han Zengyao, Ma Xingrui. Progress of spacecraft dynamics model test verification technology[J]. *Advances in Mechanics*, 2012, 42(04): 395-405.
2. He Kui, Zhang Wei, Li Changlong, et al. Thermal coupling model modification and virtual validation method for rocket strapping mechanism[J]. *Vibration and Shock*, 2024, 43(8):34-42.
3. WAN Barge, YAN Tianhong, ZHOU Guoqiang. A cantilever beam damage identification method based on modal flexibility curvature and model correction[J]. *Lifting and Transportation Machinery*, 2024(18).
4. Li, Kaiyang, Jie Fang, Bing Sun, et al. Structural Dynamic Model Updating with Automatic Mode Identification Using Particle Swarm Optimization. *Applied Sciences*12.18 (2022): 8958.
5. SHE Feng, FAN Xiaoning. Neural network-based modification of finite element model for metal structure of door machine[J]. *Computer True*, 2024, 41(10): 265-271.
6. XU Peiyuan, FENG Zhijie. Parameter correction and modal optimization of Z-pipe finite element model based on response surface method[J]. *Aircraft Design*, 2023, 43(6):30-38.
7. ZHU Xinggao, LUAN Jiahui. Structural strength analysis and validation of solar wing drive mechanism based on finite element[J]. *Computer Aided Engineering*, 2019, 28(02): 11-14.

**Open Access** This chapter is licensed under the terms of the Creative Commons Attribution-NonCommercial 4.0 International License (<http://creativecommons.org/licenses/by-nc/4.0/>), which permits any noncommercial use, sharing, adaptation, distribution and reproduction in any medium or format, as long as you give appropriate credit to the original author(s) and the source, provide a link to the Creative Commons license and indicate if changes were made.

The images or other third party material in this chapter are included in the chapter's Creative Commons license, unless indicated otherwise in a credit line to the material. If material is not included in the chapter's Creative Commons license and your intended use is not permitted by statutory regulation or exceeds the permitted use, you will need to obtain permission directly from the copyright holder.

